ON THE COMPUTATION OF WING LIFT INTERFERENCE CAUSED BY HIGH BYPASS ENGINES

ICAS-86-3.9.1

C.HABERLAND, and G.SAUER

Institut für Luft- und Raumfahrt, Technische Universität Berlin (F.R.G.)

ABSTRACT

Wind tunnel investigations with respect to optimization of commercial aircraft reveal that lift reduction due to engine interference can be significantly decreased by optimizing engine position and fan shroud contour. As a numerical approach a 3D-engine singularity method has been developed, which includes a realistic jet model. The quality and applicability of the method was tested by comparing the results (flow field, pressure coefficient, leakage) with those from the previous axisymmetric model. In order to adjust the exit velocity at the fan nozzle to the inlet flow and the fan pressure ratio, the engine singularity model was extended by an additional doublet (stator-) disc. Interference calculations on an actual research wing were performed by means of the axisymmetric engine procedure as a first step.

NOTATION

A	Matrix
$\vec{A}$	Vector potential
BC	Boundary condition
D	Nozzle diameter
E	Fan exit velocity ratio
L	Chord length
Q	Mass flow rate of fan jet
R	Radius of fan nozzle
R_o	Distance of point i from panel j
S	Surface
$\vec{V}$	Velocity field vector
$\vec{V}_\infty$	Onset flow velocity vector
$\vec{V}_i$, $\vec{V}_{tot}$	Total perturbance velocity vector
$\vec{V}_{ti}$	Tangential vector, projection of $\vec{V}_i$ to panel plane
$\vec{V}_{\infty\ ti}$	Tangential vector, projection of $\vec{V}_\infty$ to panel plane
$\vec{V}_i''$	$\vec{V}_i$ in the panel coordinate system
$\vec{V}_{iv}$	Velocity vector at virtual collocation point
$\vec{V}_{ij}$	Perturbation velocity vector in i due to panel j
$\vec{V}_z$	Entrainment velocity vector
V_N	Velocity component normal to the panel
V_R	Rotor velocity
V_S	Stator velocity
V_e	Fan exit velocity
V_o	Velocity component outside the contour
V_i	Velocity component inside the contour
a_{ij}, b_{ij}	Influence coefficients
c_{ij}, d_{ij}	Influence coefficients
c_p	Pressure coefficient
c_l	Local lift coefficient
e_x, e_y, e_z	Components of unit normal vector
$\dot{m}$	Mass flow rate
$\vec{n}$	Unit normal vector
q	Source density
$\vec{r}_{ij}$	Vector from panel j to point i
$\vec{s}$	Vector from reference system to panel coordinate system
$\vec{t}_i$	Unit tangential vector of $V_{\infty\ ti}$
$\vec{t}_x$, $\vec{t}_y$, $\vec{t}_z$	Unit vectors of panel coordinate axes
t_x, t_y	Components of $\vec{t}_i$ in the panel coordinate system
x, y, z	Reference coordinate system
z", y", z"	Panel coordinate system
x_o, y_o, z_o	Coordinates of engine position
u_{iv}, v_{iv}	Components of V_{iv}
σ	Singularity strength
$\vec{\Omega}''$	$\vec{\Omega}$ in panel coordinate system
$\vec{\Omega}$	Vortex sheet field vector in the reference coordinate system
μ	Local doublet density
β_1, β_2	Incidence angles to vertical plane
α	Angle of attack
φ	Circumferential angles
Ω_x'', Ω_y''	Components of $\vec{\Omega}''$
η	Span coordinate
φ	Perturbation potential

1. INTRODUCTION

In the design of commercial aircraft with wing-mounted engines the research concerning engine-wing interference has become increasingly more important, because inlet and exhaust flow of high-bypass engines can significantly decrease the lift on the wing when unfavourably positioned. Therefore, the reduction of engine-wing interference becomes an essential part in the aerodynamic optimization of the aircraft configuration. The majority of research undertaken concerning this problem is based on wind tunnel tests, which make up for a substantial part of the entire wind tunnel program. To cut the cost of such testing, numerical procedures are a useful tool with which parametric investigations with respect to engine geometry, position, and pylon contouring can be accomplished.

For this computation, singularity methods can be used which, however, have to be particularly adapted to the problem. To achieve this, it is necessary not only to model

an arbitrary 3D-engine geometry under variable onset flow conditions, but also to realize engine mass flow rates which have to be independent of the onset flow. Furthermore, for the simulation of the fan jet a jet model has to be attached, which allows the determination of jet propagation (-deformation, -deflection, -entrainment) as a result of the flow field induced by engine, pylon, and wing. Such an engine singularity method, when combined with a three-dimensional wing method, renders possible the pre-optimization of engine position and cowl-pylon configurations.

Detailed representations of the state of the art with respect to procedures for flow computation on engines is given in /1/, /2/, and /3/. It becomes apparent that methods which give very good results for external flow calculations show difficulties for internal flow problems, which are caused by leakage through the inner contour. As a consequence, engine mass flow rate and pressure at the contoure are falsified, Fig. 1.

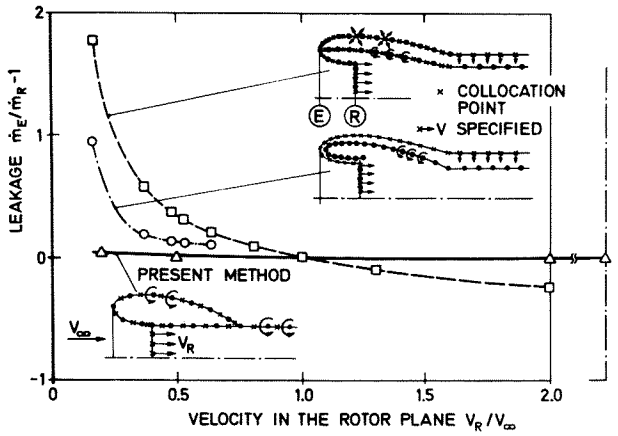

Fig. 1 Leakage Dependent on the Mass Flow Ratio for Different Singularity Models

The control of the mass flow rate by use of additional singularity sheets furthermore leads to an increase in normal velocities induced at the contour, Fig. 2.

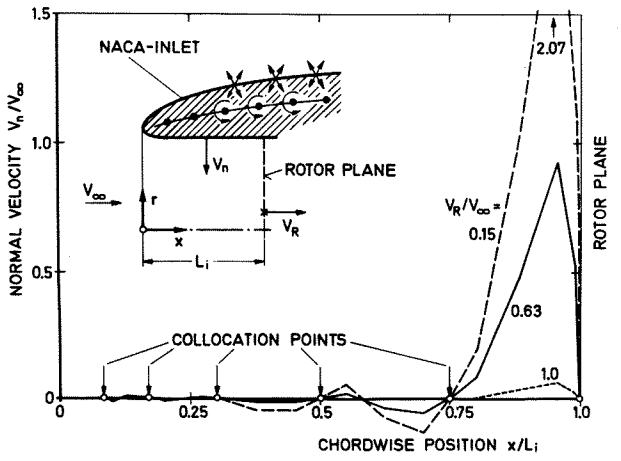

Fig. 2 Computed Leakage through the Inner Inlet Surface (acc. to Schmidt /4/)

In order to avoid these difficulties the internal engine flow is often excluded from the calculation and thus the engine is simulated by a simple displacement body. This method is restricted in general to cruise conditions in which nacelle flow and transonic wing flow play a more important role than engine inlet and exhaust flow. For transonic flow, KLEVENHUSEN, JAKOB and STRUCK /5/formulate the so-called hybrid-method, which is a combination of a panel procedure of higher order for the subsonic domain and a finite difference procedure for the transonic flow domain. ROBERTS /6/ also determines the interaction between engine jet and wing through the use of a combined procedure. The flow field is splitted into a potential flow area (airframe flow) and an area exposed to viscous flow (jet area). Using the NLR-panel method, SNEL /7/ calculates the interference effects between the engine jet and parts of the airframe on nacelle-jet-wing configurations that were also tested in a wind tunnel by KHO /8/. Very good agreement between the calculated and experimental pressure distribution on the wing is stated.

With the combination of this model and the singularity procedure VSAERO /9/, SZODRUCH /10/ examines a complete aircraft configuration in order to optimize engine position and pylon shape. He outlines the good agreement of the results with recorded data. With the use of the panel procedures of /11/ and /12/ and including viscous effects in the engine wake, RETTIE /13/ studies various wing-engine combinations. It is stressed that a pylon of conventional wing-mounted engines has an important influence on the pressure distribution of the lower side of the wing, especially inboard. The results of the panel procedure demonstrate in this area unacceptable deviations from experimental data.

Due to increased effects of the inlet and jet flow more serious interference problems occur at low flight speeds. Investigating this problem, extensive wind tunnel tests have been done for example by EWALD and SMITH /14/, BECLE and PERIN /15/, and HARRIS and CARTER /16/ using through-flow nacelles as well as turbo-powered simulators. KRENZ /17/ compares the lift distortion caused by an isolated through-flow nacelle with that of a nacelle with pylon using the measured pressure distribution on the wing. In order to achieve a pre-optimization of pylon shape and engine position and, thereby, a cutting of cost for wind tunnel tests, he recommends the use of theoretical methods.

HAFTMANN and KIEKEBUSCH /18/ argue that the increasing amount of wind tunnel tests in the aerodynamical development of the Airbus A320 (approximately twice that of the A310 development) is due to the economical necessity for performance optimization. This is caused particularly by the increase of the interference due to the use of high-bypass engines. From the interpretations of the wind tunnel tests with variable engine position, nozzle length, and pylon shape it appears to be possible to compensate for the local lift loss on the wing by lift generated by the nacelle due to the up-wind field of the wing.

The jet calculation method from SNEL /19/ (which is used in the panel method presented in this paper) is based on a VTOL-jet model for the calculation of a jet in uniform cross flow. Extended to arbitrary flows it allows a three-dimensional jet computation in a non-uniform flow field, taking into account both wing and nacelle flow. The state of the art of engine-jet-airframe interference is further outlined by BARCHE /20/. He comments that methods based on potential theory alone are not sufficient, especially for the jet calculation in the case of small engine-wing distances. On the other hand, computation methods that include viscosity are restricted because of difficulties in the evaluation of 3D-turbulent shear-layers and intermittency effects.

For the investigation of axisymmetric bypass engines a panel method is presented in /1/, which, contrary to the

conventional source-sink arrangement, uses a singularity model where vortex sheets and doublets are located on the contour. Through the combination of these singularity types with suitable boundary conditions tangential and normal to the contour the flow inside the cowl is suppressed. Leakage due to internal engine flow and mass flow actuating disc is therefore insignificant, Fig. 1. The extension of the procedure to an evaluation of the interference effects between engine and rectangular wings is demonstrated for varying engine position, angle of attack, and mass flow rate in /3/. The results have to be seen as a first approximation of the interference problem, because by using an axisymmetric engine model the influence of the wing on the engine cannot be correctly accounted for. Therefore, on the basis of this axisymmetric procedure a 3D-engine singularity method has been developed. It can be shown that covering the surface with vortex sheets and doublets leads to adequate suppression of the flow inside the contour and to the conservation of mass in the engine through-flow even in 3D-geometries.

2. THREE-DIMENSIONAL SINGULARITY METHOD

2.1 Concept of the Vortex-Doublet Method

A singularity model for a 3D-engine panel procedure has been developed, Fig. 3, which describes the engine contour by partial doublet sheets and a bound vortex layer with variable circulation along chord and circumference, leading to free vortices in flow direction. The unknown circulation is determined by the Kutta-point (collocation point of the additional panel downstream the trailing edge) as well as by the tangential boundary condition at the interior of the contour. This approach renders possible to suppress the flow within the fan shroud.

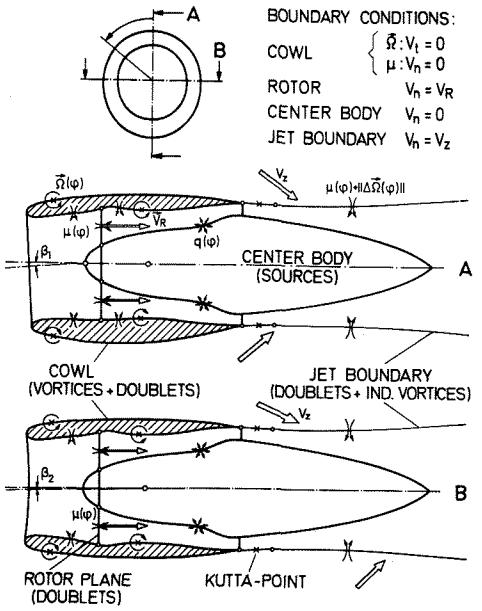

Fig. 3 Singularity Model of a 3D-Engine-Jet Geometry

Control of the mass flow rate is accomplished by means of the use of a doublet-covered rotor disc, by which the velocity through the rotor plane can be varied. This velocity is used as the reference velocity for the total system and, set in relation to the onset flow velocity, provides a measure for the mass flow rate. However, the use of the rotor disc induces strong normal velocity components on the internal contour of the cowl which cannot be suppressed by means of the tangential boundary condition alone. Therefore an additional variable doublet covering is provided the intensity of which being dictated by the conventional boundary condition normal to the panel. For this region both the tangential and normal velocity components are suppressed at the same time.

Mathematical Background

After determining the singularity intensity by solving the FREDHOLM integral equation of second kind

$$2\pi q_i - \oiint_S \frac{\partial}{\partial n}\left(\frac{1}{r_{ij}}\right) q_j \, dS = -\vec{V}_\infty \vec{n}_i \,, \qquad (1)$$

the flow field can be calculated. This integral equation is formulated here for the perturbation potential of a body which surface is continuously covered with sources

$$\varphi(r) = \oiint_S \frac{q_j}{r_{ij}} \, dS \qquad (2)$$

with the condition that the normal derivative of the *complete* flow potential (onset flow potential and perturbation potential) disappears:

$$\left.\frac{\partial \varphi}{\partial n}\right|_S = \vec{n} \operatorname{grad} \varphi \Big|_S = -\vec{n}\vec{V}_\infty \Big|_S \,. \qquad (3)$$

Through discretization of the surface by flat panels which, corresponding to HESS and SMITH /21/, are assumed to have constant singularity strength and by satisfying the kinematic flow condition at the defined collocation points on each panel, the FREDHOLM-integral can be approximated by a system of linear equations with which the unknown singularity intensities can be computed.

Induced Velocities

The velocity field of an arbitrary displacement body can be represented as the gradient of the potential function $\varphi(r)$

$$\vec{V}(r) = -\operatorname{grad} \varphi(r) \qquad (4)$$

The induced velocities due to a source distribution of constant intensity results from the derivative of the perturbation potential, Eq. (2). Choosing a constant doublet distribution on the panel with the doublet axis normal to the surface instead of the sources yields the components of the induced velocities also from Eq. (2)

$$\varphi_{Dij} = -\frac{\partial \varphi_{ij}}{\partial z} = -V''_{Zij} \,. \qquad (5)$$

In order to determine the induced velocities due to a constant vortex sheet on the panel, the velocity field $\vec{V}$ is expressed as the rotation of another vector field $\vec{A}$, which can be computed using the field vector of the vortex sheet $\vec{\Omega} = (\Omega''_x, \Omega''_y, 0)$ /21/. Hence, the induced velocity at an arbitrary point of the field is, Fig. 4a,

$$\vec{V}''_i(r) = \operatorname{curl} \vec{A}''(r) = \operatorname{curl} \oiint_S \frac{\vec{\Omega}''_j}{r_{ij}} \, ds \,. \qquad (6)$$

Since the intensity of the vortex sheet is constant, $\vec{\Omega}''$ can be taken in front of the integral and the vector potential $\vec{A}$ yields in the coordinate system of the panel

$$\vec{A}''(r) = \vec{\Omega}_j'' \iint_S \frac{1}{r_{ij}}\, ds \qquad (7)$$

The integral therefore corresponds to the perturbation potential φ in Eq (2). Written in components, the relation for the induced velocity is

$$\vec{V}''(r) = \mathrm{curl}\left[\left(\Omega_x''\varphi\right)\vec{t}_x + \left(\Omega_y''\varphi\right)\vec{t}_y + 0\,\vec{t}_z\right] \quad . \qquad (8)$$

In panel coordinates the induced velocity components due to the constant vortex sheet are

$$\begin{aligned} V_{xij}'' &= -\Omega_{yj}'' \frac{\partial\varphi}{\partial z}\, ij \quad , \\ V_{yij}'' &= \Omega_{yj}'' \frac{\partial\varphi}{\partial y}\, ij \quad , \\ V_{zij}'' &= \Omega_{yj}'' \frac{\partial\varphi}{\partial x}\, ij - \Omega_{xj}'' \frac{\partial\varphi}{\partial y}\, ij \quad . \end{aligned} \qquad (9)$$

The solution of the system is obtained according to /21/. The components of the vortex vectors Ω_x'' and Ω_y'' are the unknown variables.

Boundary Conditions and Equation System

The representation of the engine surface by vortex sheets and partially by doublets leads to a suppression of the internal field. The tangential velocity in an arbitrary point of the contour is then equal to the vortex intensity, because of $V_a - V_i = \|\vec{\Omega}\|$, when the internal flow vanishes. Since a constant vortex does not induce a normal velocity in its own collocation point, it is required that the velocity component tangential to the panels must be zero, in order to suppress the flow inside the contour. By this measure it can be achieved that the panel's self-induced tangential velocity, which represents the largest part of the induced total velocity, à priori disappears. Then, the boundary condition analogous to Eq. (3) is

$$\vec{V}_{\infty ti} + \vec{V}_{ti} = 0 \quad . \qquad (10)$$

$\vec{V}_{\infty t}$ and $\vec{V}_{ti}$ are the tangential vectors of $\vec{V}_\infty$ and $\vec{V}_i$ projected onto the panel plane i, Fig. 4b. Through the use of sources and doublets the vanishing normal components of the onset and perturbation velocity in the panel collocation points is prescribed. For this to be the case, the normal components of the onset flow and the perturbation velocity must be of the same magnitude and in opposite direction.

Applying source and doublet distributions, and the boundary condition normal to the panel, the fullfillment of the kinematic flow condition on the contour becomes dependent on the determination of one unknown variable per panel only which is its source/doublet intensity

$$\begin{aligned} &\sum_{j=1}^{N} a_{ij}\cdot\sigma_j = -\vec{V}_\infty \vec{n} \quad ; \quad i = 1, \ldots N \\ &a_{ij} = \vec{V}_{i,j}\cdot\vec{n}_i \quad , \end{aligned} \qquad (11)$$

Contrary to this, through the use of vortex sheets in connection with a tangential boundary condition, the tangential vector $\vec{V}_{ti}$ of the total perturbation velocity has to be determined not only in its magnitude, but also in its direction in order to meet the kinematic flow condition. In doing so, the components of the vortex sheet of the field vector of the inducing panels $\vec{\Omega}_j = (\Omega_{xj}'', \Omega_{yj}'')$ represent the unknown variables, which can be evaluated from a system of 2N equations for N different panels, Fig. 5. The equation system to satisfy the tangential boundary conditions, Eq. (10), is

$$\begin{aligned} \vec{V}_i \cdot \vec{t}_{xi} &= \sum_{j=1}^{N} \left(a_{ij}\,\Omega_{xj} + b_{ij}\,\Omega_{yj}\right) = -\vec{V}_\infty \vec{t}_{xi} \\ \vec{V}_i \cdot \vec{t}_{yi} &= \sum_{j=1}^{N} \left(c_{ij}\,\Omega_{xj} + d_{ij}\,\Omega_{yj}\right) = -\vec{V}_\infty \vec{t}_{yi} \quad . \end{aligned} \qquad (12)$$

The portion of the self-induced velocity of the total perturbation velocity is

$$\vec{V}_{i,i} = \vec{V}_{INSIDE} = \begin{pmatrix} -2\pi\,\Omega_x \\ 2\pi\,\Omega_y \\ 0 \end{pmatrix} \quad . \qquad (13)$$

The 2N x 2N equation system for the computation of the vortex distribution on the engine cowl can be coupled with conventional N x N systems, and as such for the engine singularity model illustrated in Fig. 3 can be solved.

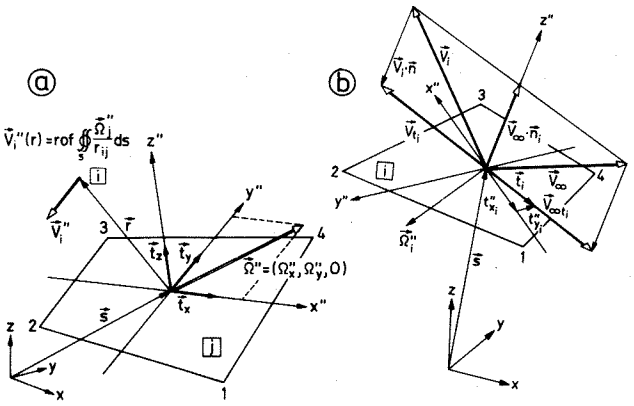

Fig. 4 Induced Velocity due to a Constant Vortex Sheet on the Panel (a), Tangential and Normal Boundary Conditions (b)

$$\begin{bmatrix} a_{11} & b_{11} & a_{12} & b_{12} & a_{13} & b_{13} & \cdots \\ c_{11} & d_{11} & c_{12} & d_{12} & c_{13} & d_{13} & \cdots \\ a_{21} & b_{21} & a_{22} & b_{22} & a_{23} & b_{23} & \cdots \\ c_{21} & d_{21} & c_{22} & d_{22} & c_{23} & d_{23} & \cdots \\ \vdots & & & & & & \end{bmatrix} \cdot \begin{bmatrix} \Omega_{x_1} \\ \Omega_{y_1} \\ \Omega_{x_2} \\ \Omega_{y_2} \\ \vdots \end{bmatrix} = \begin{bmatrix} V_\infty t_{x_1} \\ V_\infty t_{y_1} \\ V_\infty t_{x_2} \\ V_\infty t_{y_2} \\ \vdots \end{bmatrix}$$

Fig. 5 Set of Equations for the Calculation of the Vortex Intensity on the Fan Cowl

The solution yields the actual source, vortex and doublet intensities, which generate the desired contour. Thus, the velocity in each point in the flow field can be determined through the summation of the onset flow and the perturbation velocities induced by all panels

$$\vec{V}_{tot\,i} = \sum_{j=1}^{N} \vec{V}_{i,j}\cdot\sigma_j + \vec{V}_{\infty i} \qquad i = 1, \ldots N \quad . \qquad (14)$$

From the total velocity results the pressure coefficient for incompressible flow

$$c_{pi} = 1 - \left(\frac{V_{tot\,i}}{V_\infty}\right)^2 \quad . \qquad (15)$$

Selected Jet Model

For coupling to the 3D-engine panel procedure, only those jet models are applicable which allow an allocation of singularities on the jet boundary, which - via the boundary condition - permits the local control of the entrainment. Furthermore, a type of singularity (doublet or source) must be used with which entrainment can be simulated. For this reason jet models which are based on a singularity distribution on the jet axis /23/ are not appli-

cable. Equally, procedures must be rejected which use vortex sheets or vortex annulars on the jet contour, because they consider only the displacement effect of the jet /24/, and no entrainment. Besides that, the jet model must be able to consider the effect of a nonuniform flow field on the jet propagation caused by the influence of the engine cowl, the inlet flow, and the flow around the wing. These requirements are met to a large extent by the integral method of SNEL /25/ which bases on the concept of two domains, the potential - core region and the fully developed region, and provides a semi-empirical relation for the calculation of the jet entrainment. The background of this method is outlined in /26/.

The 3D-engine procedure should allow the adjustment of an engine mass flow which is independent of the onset flow. This renders possible the generation of arbitrary fan exit velocities as initial condition for the jet. The jet is, therefore, part of the total flow field and can no longer be considered as an isolated sink as in the case of a pure blown nacelle. Consequently, for the realization of the jet entrainment in the singularity method, instead of sinks (NLR-panel procedure) doublets allocated on the jet surface are used, which allow a continous flow through the jet boundary so that the increase in jet mass flow can be simulated. The entrainment function which has been applied as boundary condition is given in /26/.

2.2 Engine-Wing-Configuration

An industrial wing panel method of higher order /27/ which approximate the wing contour through the use of curved panels is used for the calculation of the interference on an actual engine-wing configuration. The set of linear equations, which determines the mutual interference of engine and wing, is outlined in Fig. 6. In the special case of an axisymmetric method being used for calculating the engine, 3D-induction effects of the wing on the engine cannot be taken into account, and the equation system simplifies as shown in Fig. 6 . The influence coefficients of the engine onto the wing can be taken from Fig. 7. The calculation is carried out by

$$\begin{bmatrix} A_E & A_{W-E} \\ A_{E-W} & A_W \end{bmatrix} \cdot \begin{bmatrix} \sigma_E \\ \sigma_W \end{bmatrix} = \begin{bmatrix} BC_E \\ BC_W \end{bmatrix}$$

FOR $A_{W-E} \equiv 0$:

$$\sigma_W = A_W^{-1} \left[BC_W - A_{E-W} \cdot A_E^{-1} \cdot BC_E \right]$$

Fig. 6 Computation of the Singularity Strengths on the 3D-Wing

computing the perturbation velocity in virtual collocation points of the engine coordinate system, transformation of the perturbation velocity into the real wing collocation points, and multiplication with the normal unit-vectors of the wing. The change of the boundary conditions, Fig. 6, can be interpreted as a virtual wing twist in that part of the wing where the flow is influenced by the engine.

3. COMPUTATIONAL RESULTS

3.1 Verification of the Jet Model

In order to check the quality of the modified jet singularity model, an engine-wing configuration, Fig. 8, is examined that was used for the NLR wind tunnel tests /8/and computations with the NLR panel method. In Fig. 9a the NLR blown nacelle is shown which for the ILR panel method /1/ was replaced by a geometrically corresponding through flow nacelle with actuated mass flow.

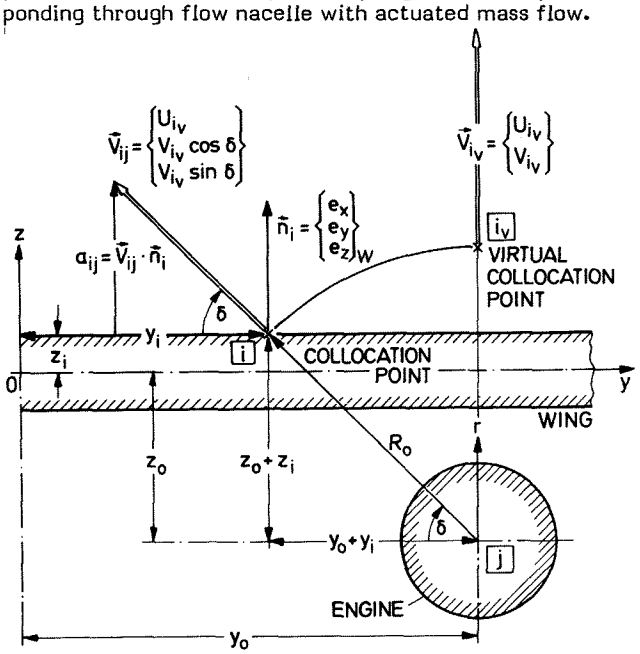

Fig. 7 Determination of Influence Coefficients on the Wing

Applying this method to the NLR-configuration, the pressure distributions in different wing sections were computed and compared with those obtained by KHO /8/.

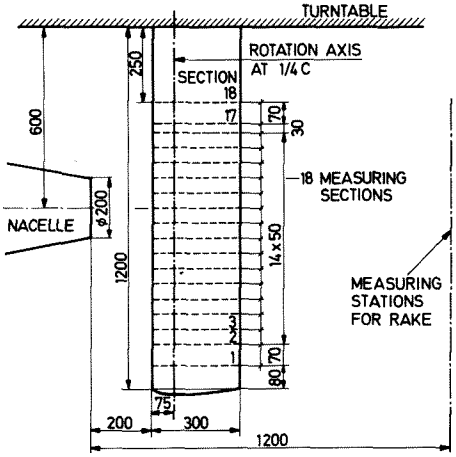

Fig. 8 Wing-Nacelle Configuration of NLR Wind Tunnel Test

Due to the 2D-wing model applied in this calculation the pressure distributions at the respective spanwise positions are symmetric to the span coordinate at engine position, e.g. sections 8 and 14 in Fig. 8. Close to this "engine-section" the calculated pressure coefficients compare reasonably well the measured ones, Fig. 9a to c.

In order to apply the computational procedure to engine geometries which are more realistic than the blown nacelle the propagation of a fan jet of a high-bypass engine (μ = 6) was investigated. In Fig. 10a and b, the development of jet mass flow ratio and normalized jet radius are plotted for different fan exit velocity ratios E.

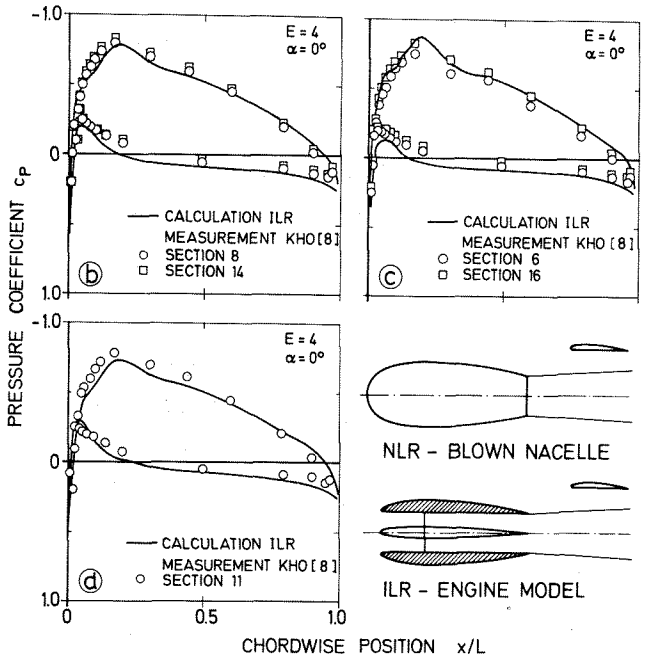

Fig. 9 NLR Wind Tunnel Configuration. Comparison of Calculated to Measured Pressure Distributions

The influence of the onset flow velocity on the jet contour becomes more obvious in Fig. 11, where for a discretized engine-jet configuration the change of potential-core length and jet expansion is shown.

Corresponding to the investigations in an uniform flow field, the jet characteristics were calculated for the engine-wing configuration in Fig. 12a, for different angles of attack and engine mass flow rates. For both uniform and non-uniform flow, the jet axes show nearly straight patterns, Fig. 12b.

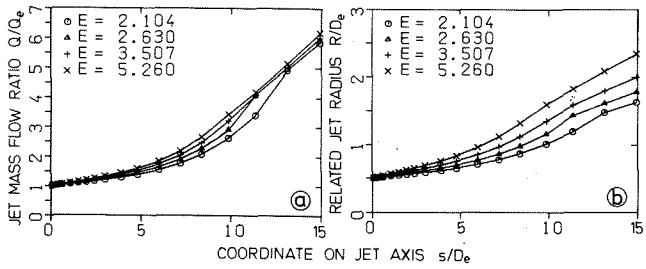

Fig. 10 Jet Mass Flow Rate (a) and Radius (b) in Uniform Flow Field, Depending on Fan Exit Velocity Ratio

3.2 3D-Engine Calculation Method

Comparison with Axisymmetric Computation

For the examination of the program system with respect to coordination of the singularity types and boundary conditions, flow field computations with the 3D-engine panel method were performed on an axisymmetric engine-jet-configuration, for which results from earlier computations /1/ existed. This comparison became necessary, because no experimental data for isolated nacelles were available. In the following examples a simple empirical jet model /1/ is used, in order to allow this comparison.

The resulting velocity fields of the 3D-method are shown in Fig. 13 for axisymmetric onset flow and mass flow ratios of $V_\infty/V_R = 0$ and 0.4, respectively. They show vanishing velocity components inside the cowl and, consequently, a tangential flow around the contour. Therefore, it is to be expected that with a 3D-program system results can be obtained which, inspite of the circumferential discretization, favourably compare to those of an in peripheral direction mathematically more exact axisymmetric method.

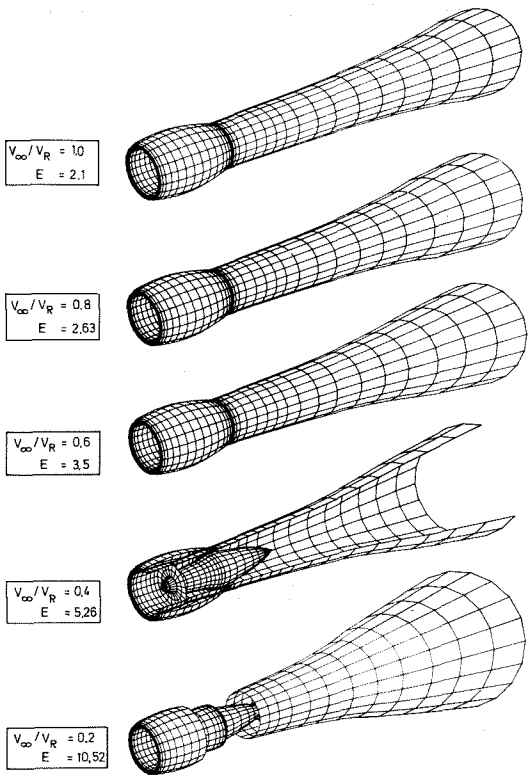

Fig. 11 Jet Geometry, Depending on Onset Flow Velocity Ratio

Furthermore, the pressure distribution on the cowl was calculated and the results compared with those of the axisymmetric panel method /1/, Fig. 14a and b. For the onset flow ratio $V_\infty/V_R = 0.4$ the comparison yields a

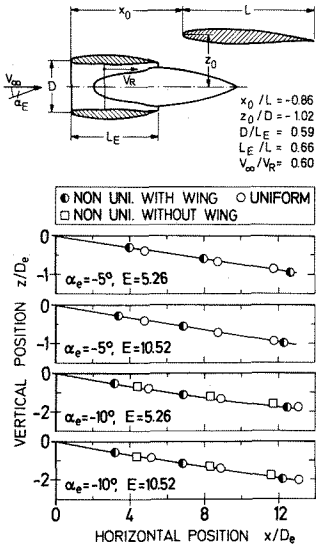

Fig. 12 Jet Axis Deflection in Uniform and Non-Uniform Flow Field

nearly complete agreement within the inlet and on the outside of the shroud contour, Fig. 14b. The small deviation on the inside of the cowl inlet lip and in the region of the fan nozzle are caused by geometric differences, which arise from the 3D-surface discretization. For the more extreme static thrust condition ($V_\infty / V_R = 0$) a different stagnation point position is calculated with the 3D-computation, Fig. 14a. In comparison to the axisymmetric computation, this point is located nearer to the inlet lip. The pressure distribution shows a deviation near the fan nozzle only.

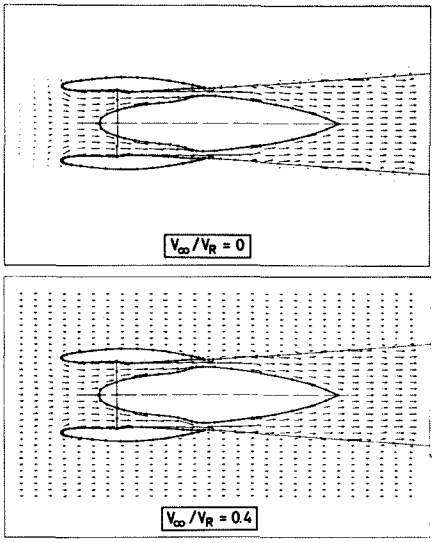

Fig. 13 Computed Flow Field of a Bypass Engine

In order to make a quantitative statement about the conservation of mass of the engine throughflow, which the velocity fields does not provide, an additional calculation of the leakage was made. This is effectively done through determining the normal velocity components normalized by the rotor velocity (V_N/V_R), Fig. 14c, d. This ratio is a measure of the

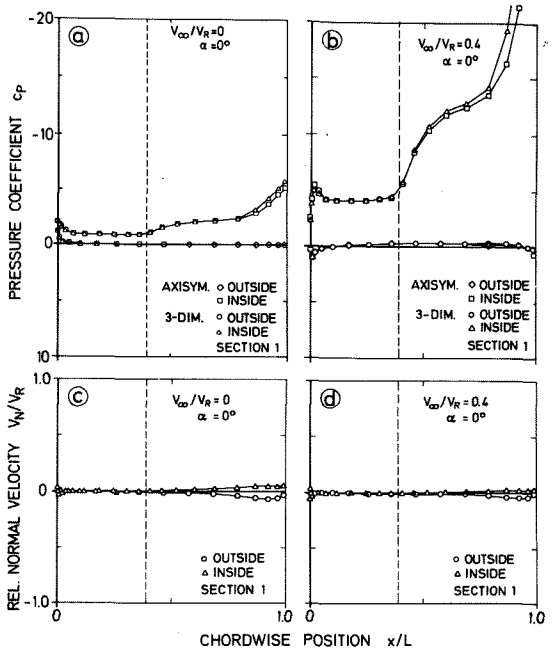

Fig. 14 Comparison of Axisymmetrically and 3D-Computed Fan Cowl Pressure Distribution (a, b). Leakage for 3D-Method (c, d).

error in the computation of the tangential velocity. The maximum local error is around 7 % for the static thrust condition (chord position x/L = 0.9). In comparison, for the other flow condition the error is below 1 %.

Application to Non-Axisymmetric Engines

Having tested the method on an axisymmetric engine, a more realistic engine geometry was provided by means of an industrial data set for the Airbus A300-configuration. In order to optionally reduce the size of the engine

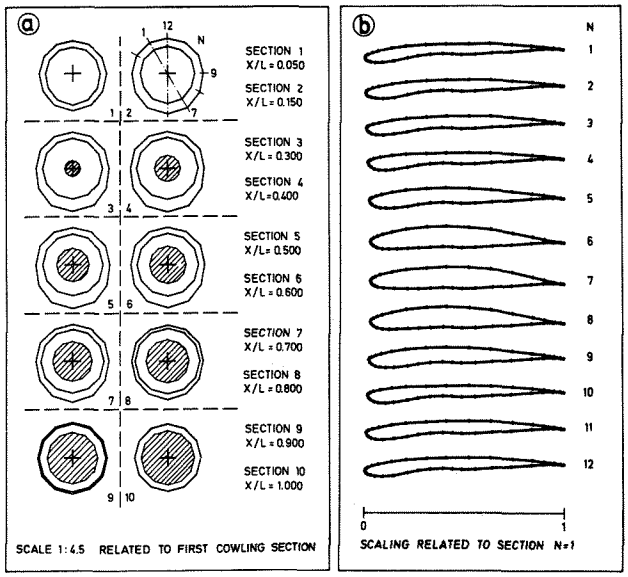

Fig. 15 Engine Cross Sections (a) and Fan Cowl Sections (b)

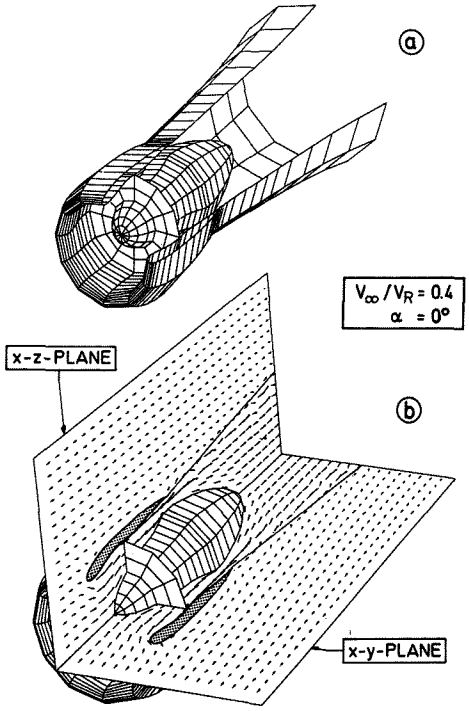

Fig. 16 3D-Engine Model (a) and Computed Velocity Field (b)

coefficient matrix the cross sections of the 3D-engine geometry were approximated by means of a spline-inter-

polation, and discretized symmetrically to the X-Z-plane Fig. 15a. The respective profile sections are shown in Fig. 15b. Coupling this geometry with a jet model data set which corresponds to the required flow conditions (flight velocity and mass flow rate) yields the complete data input for the engine program system.

First, the flow fields of this modified A300-engine geometry for an onset flow velocity ratio $V_\infty / V_R = 0.4$ and different angles of attack are determined. In order to demonstrate the 3D-engine flow, a perspective view of the engine model is shown in Fig. 16a, and the velocity field in the X-Y plane and X-Z plane of the engine coordinate system is plotted for the velocity ratio 0.4 and zero angle of attack in Fig. 16b. This way, arbitrary perspectives of 3D-computed velocity fields can be drawn in one plot and directly associated with the engine configuration. Fig. 17 shows the flow field and the streamline pattern in the X-Z-plane of the engine for the velocity ratio $V_\infty / V_R = 0.4$ and an angle of attack $\alpha = 3°$. Due to

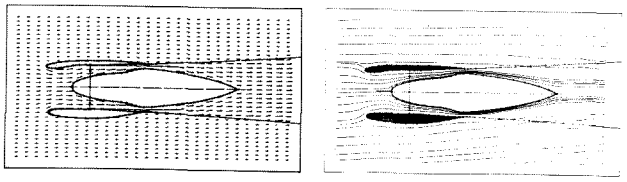

Fig. 17 Velocity Field and Streamlines. Angle of Attack 3 deg., Onset Flow Velocity Ratio 0.4

the incidence, a larger jet entrainment is produced on the windward side of the engine jet. The entrainment on the lee-side affects the streamlines also in the outer flow field to be deflected towards the engine jet. The computed pressure distributions in the corresponding collocation points of the cowl section 1 and 6 (Fig. 15a)

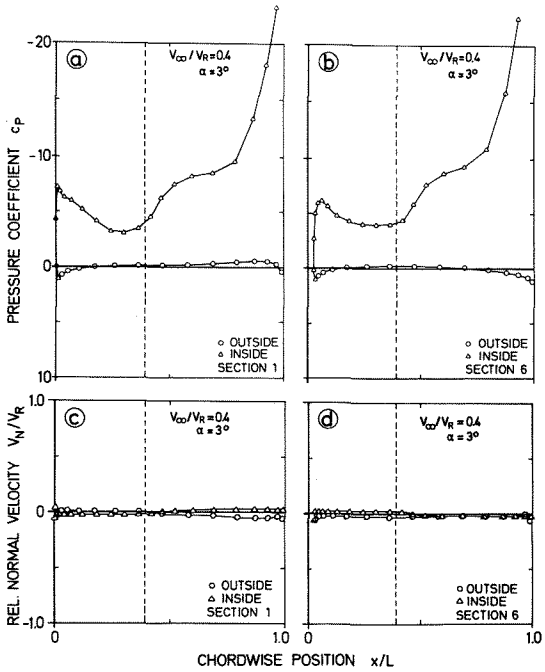

Fig. 18 Computed Pressure Distribution and Leakage at two Cowling Sections

are shown in Fig. 18. They outline the differences in the flow along the respective sections varying in peripherial direction. The flow around the very slim upper profile (section 1) yields a pronounced pressure peak at the leading edge, which is quickly reduced in the inlet due to the camber of the profile contour. As can be seen from the pressure distribution, the flow approaches the prescribed through-flow boundary condition immediately in front of the rotor plane. Within the inlet, regions of very low pressure occur, which govern the pressure distribution on the outer contour, Fig. 18a. Thereby, they essentially contribute to the aerodynamic loads on the nacelle.

In comparison to cowl section 1, the flow around the lower section 6, Fig. 18a, yields due to the inclination of the engine highlight, the larger profile thickness, and the non-cambered inlet contour a weaker flow acceleration, and therefore, a lower pressure peak at the leading edge. Obviously, highlight inclination and different contouring result in an insensibility of the engine to small angles of attack. For the angle of attack $\alpha = 3°$ the leakage can be neglected at the whole cowl contour, as demonstrated in Fig. 18c and d.

3.3 Engine-Wing-Interference

In order to check the flow computations by means of comparable aerodynamic data, a data set of an A310-experimental wing /28/ (chord length -, thickness-, twist distribution) has been applied for the generation of the wing geometry. To illustrate wing geometry and engine position, the discretized engine-wing-configuration is plotted in Fig. 19. To verify correct geometry generation, the wing lift, at first, was calculated without engine influence, and then compared to the lift distribution according to /28/, Fig. 20a. Small deviations occur only at the trailing edge, where no sufficient geometry data had been available.

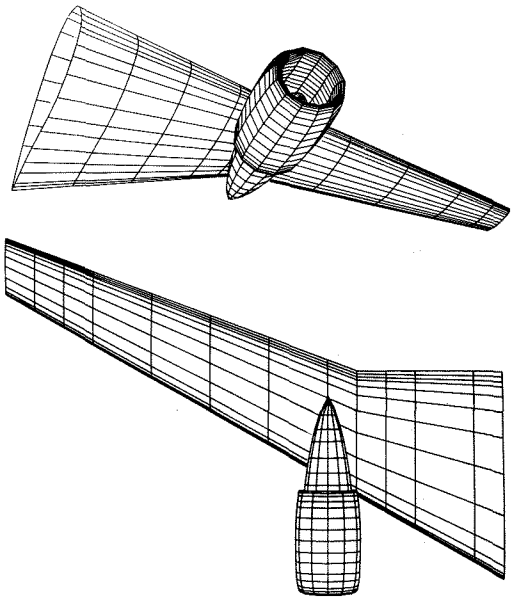

Fig. 19 Discretized Engine-Wing Configuration (Airbus Experimental Wing)

To evaluate the interference effect caused by the engine, the complete configuration was investigated at velocity ratios $V_\infty / V_R = 0.6$ (take-off) and 1.0 (cruise) with constant angle of attack (engine: 0°, wing: 2°). For simplicity, in this first approach the actual engine was idealized by an axisymmetric engine model. The resulting pressure distribution on the wing section at engine position is compared with that of the clean wing, Fig. 20b. It becomes evident that the flow around and through the engine affects mainly the front half of the profile only. On the lower side of the wing, a pressure reduction

occurs, which increases with growing mass flow rate. On the upper side, the acceleration of the flow between engine cowl and wing leads to a reduction of the suction peak at the leading edge with increasing mass flow. The pressure distribution on the rear part of the section, in comparison, is only slightly affected by the engine flow.

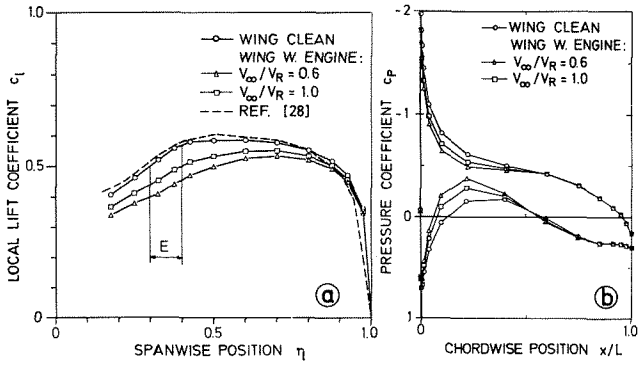

Fig. 20 Lift Distribution (a) and Pressure Distribution (b) of a Experimental Wing. Comparison Clean Wing to Wing-Engine Configuration

The lift distribution along the wing span for both velocity ratios can be seen in Fig. 20a. It is obvious that the lift decay is noticeable over the total wing span. Compared to the clean wing, the loss of integrated wing lift is around 12 % for V_∞/V_R = 0.6 and about 7 % for 1.0. The lift distribution in cruise flight agrees qualitatively well with that cited in /29/. There, the lift loss for a flight Ma-number 0.78, which was computed with the hybrid-method, is specified with 5.3 %.

4. EXTENDED ENGINE MODEL

In order to allow control of the exit velocity at the fan nozzle, the engine singularity model was modified: Just behind the rotor plane a further doublet disc was installed by means of which - corresponding to the boundary condition in the rotor plane - the flow velocity through this plane can be preset. This results in a "stator/rotor" velocity ratio which adjusts the fan exit velocity to the flight condition and the fan pressure ratio. The boundary condition for this second disc (stator velocity) was derived from fan performance maps, e.g. the correlation of fan exit velocity to flight Ma-number and fan pressure ratio. Actually, this pressure ratio changes with the particular flight condition (e.g. the GE CF6-80-a1 engine: cruise Π_F = 1.76, max. take-off - Π_F = 1.68).

The concept of a stator aims at the adjustment of a correct fan exit velocity ratio taking into account the change in flow cross section along the fan channel as well as compressibility. Since in the discussed panel method hereto no compressibility correction is implemented, this adjustment is made assuming a constant fan pressure ratio. To outline the effect of this velocity ratio on the jet propagation and the flow through the engine as well as to demonstrate the feasibility of the concept in principle, 3D- and axisymmetric computations of the flow field with a fan pressure ratio 1,75 were performed for two flight conditions. In Fig. 21 the flow field and the pressure coefficient for the axisymmetric engine are shown for 2 different mass flow ratios. The figure indicates that the jet expansion decreases with increasing onset flow velocity. Downstream, the velocity within the jet approaches that of the outer field, Fig. 21a. Furthermore, the velocity vectors at the fan exit underline that for both flight cases the initial condition E for the jet is correctly adjusted with the rotor/stator velocity ratio, and the exit velocity increases with decreasing E (increasing V_∞/V_R).

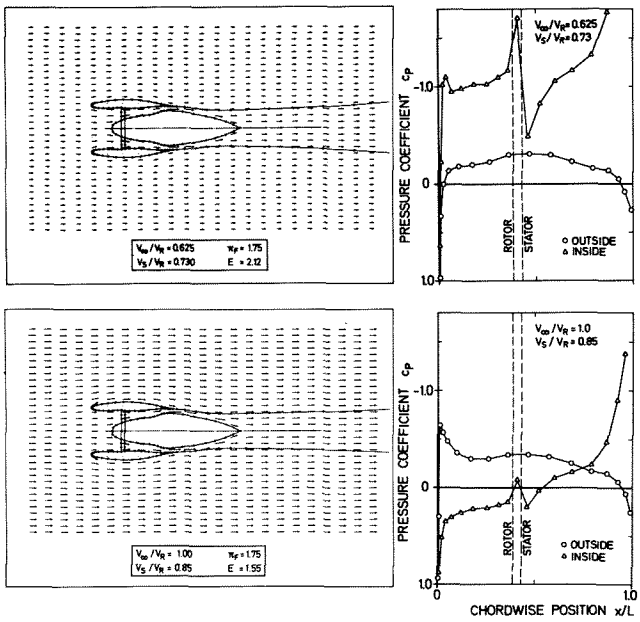

Fig. 21 Computed Velocity Fields and Pressure Distributions at the Fan Cowl, Dependent on Rotar-Stator Velocity Ratio

This is confirmed by the pressure distribution inside the fan shroud, Fig. 21b. The inlet pressure distribution is governed, as in the case without stator, only by the mass flow ratio. Immediately behind the rotor plane, however, the stator doublets give rise to a pressure step. At the leading edge the pressure distribution shows a peak which is typical for this velocity ratio. This peak decreases with increasing onset flow velocity. In the same way the pressure rise in the stator plane decreases since it is controlled by the adjusted initial jet condition.

5. FUTURE DEVELOPMENTS

The discussed panel method, which bases on the concept of a combined vortex-doublet singularity formulation for the engine and the jet, appears to be capable to provide reasonable, practical results. In particular, the implementation of an additional stator disc can be expected to result in an efficient method for flow field calculations, interference prediction and, thereby, pre-optimization of engine position as a preliminary step to wind tunnel tests. However, it was felt that it would be desirable to extend the program system to a more general application to design optimization (which includes optimization of the cowl and pylon contour). Therefore, efforts for the following subjects are in progress:

- Although the axisymmetric engine model yields results in good agreement with those of industrial computations, the applied wing method has to be coupled with the developed 3D-engine module. This work will be promoted because only with this combined method the influence of the wing on the fan cowl in the coefficient matrix can be taken into account and, furthermore, a pylon module can be attached.

- The resultant lift distribution of the wing was calculated without pylon. It is well known, that pylon flow leads to a more peaky lift distribution near the engine compared to the more equalized distribution discussed in Fig. 21b. Therefore, a pylon module will be added.

- For a more easy handling of the program system a monitoring program should be developed which provides preprocessing, program control, postprocessing, and data flow as well as storage organization.

- Finally, the data input should be actualized by means of fan stage performance maps of actual high bypass-engines and/or turbo-powered simulators.

ACKNOWLEDGEMENT

The authors are grateful to M. KARWIN and R. STOER for their assistance in the computational work and in preparing this paper. This research was supported by the German Science Foundation.

REFERENCES

/1/ Haberland, C., Göde, E., Sauer, G.: "Calculation of the Flow Field Around Engine-Wing Configurations", ICAS-Paper No. 80-4.1, Proc. 12th ICAS-Congress, Munich, 1980

/2/ Sauer, G., Haberland, C.: "Ein potentialtheoretisches Verfahren zur Berechnung der Umströmung von V/STOL-Triebwerken und Triebwerk-Flügel-Konfigurationen bei beliebiger Anströmung", ILR-Mit. 89, Institut für Luft- und Raumfahrt, TU-Berlin, 1981

/3/ Sauer, G., Haberland, C.: "Beiträge für ein dreidimensionales Singularitätenverfahren zur Berechnung der Triebwerk-Flügel-Interferenz", ILR-Mit. 128, Institut für Luft- und Raumfahrt, TU-Berlin, 1983

/4/ Schmidt, W.: "Potentialtheoretische Berechnungsverfahren für Unter- und Überschallströmung. Ein kritischer Überblick", Bericht 74/54b, Dornier, 1974

/5/ Klevenhusen, K.D., Jakob, H., Struck, H.: "Calculation of Wing-Body-Nacelle Interference in Subsonic and Transonic Flow", AGARD CP-301, Mai, 1981

/6/ Roberts, D.W.: "Prediction of Subsonic Aircraft Flows with Jet Exhaust Interaction", AGARD-CP-301, 1981

/7/ Snel, H.: "Evaluation of a Method for the Prediction of Jet Airframe Interference", NLR TR 76131 U

/8/ Kho, Y.G.: "Wing-tunnel Measurements on the Interference between a Jet and a Wing, Located Outside the Jet", Part I, NLR TR 77 009U

/9/ Maskew, B.: "PROGRAM VSAERO. A Computer Program for Calculating the Non-Linear Aerodynamic Characteristics of Arbitrary Configurations", User's Manual, 1982

/10/ Szodruch, J.: "Integriertes Flügel-Antriebs-System (IFAS)", - Phase II - BMFT-FB-W85-008, Juni 1985

/11/ Rubbert, P.E., Saaris, G.R.: "Review and Evaluation of a Three Dimensional Lifting Potential Flow Analysis Method for Arbitrary Configurations", AIAA-Paper No. 72-188, San Diego, 1972

/12/ Gilette, W.B.: "Nacelle Installation Analysis for Subsonic Transport Aircraft", AIAA-Paper No. 77-102, L.A. Cal. 1977

/13/ Rettie, I.H.: "Interference Problems in Aircraft Design", AGARD-FDP Special Course, Mai 1983

/14/ Ewald, B., Smyth, R.: "The Role and Implementation of Different Nacelle/Engine Simulation Concepts for Wind-Tunnel Testing in Research and Development Work on Transport Aircraft", AGARD-CP-301, Mai 1981

/15/ Becle, J.P., Perin, R.: "Essais en soufflerie de maquettes motorisées comparaison de deux de simulation des jets des réacteurs", AGARD-CP-301, 1981

/16/ Harris, A.E., Carter, E.C.: "Wind Tunnel Test and Analysis Technique Using Powered Simulators for Civil Nacelle Installation Drag Measurement", AGARD-CP-301, Mai 1981

/17/ Krenz, G.: "Engine/Airframe Interference", AGARD-FDP-VKI, Special Course, Mai 1983

/18/ Haftmann, B., Kiekebusch, B.: "Details zur Optimierung des Reiseflugwiderstands des Airbus A320", DGLR-Nr. 85-89, Jahrestagung der DGLR, Bonn-Bad Godesberg, 30. Sept. - 2. Okt. 1985

/19/ Snel, H.: "The Interaction between a Jet and a Non-Uniform Mainflow, and Jet-Airframe Interaction", NLR MP 75019 U

/20/ Barche, J.: "Jet Interaction with Neighbouring Surfaces", AGARD-CP-308, Lissabon, 1982

/21/ Hess, J.L., Smith, A.M.O.: "Calculation of Potential Flow About Arbitrary Bodies", Progress in Aeronautical Science, Vol. 8, Pergamon Press, London, New York, Paris, 1967

/22/ Karamcheti, K.: "Principles of Ideal-Fluid-Dynamics", John Wiley and Sons, Inc. New York, London, Sydney 1967

/23/ Wooler, P.T., Burghart, G.H., Gallagher, J.T.: "Pressure Distribution on a Rectangular Wing with a Jet Exhausting Normally into a Cross Flow", J. Aircraft, Vol. 4, No. 6, 1967

/24/ Shollenberger, C.A.: "Three-Dimensional Wing/Jet Interaction Analysis Inducing Jet Distortion Influences", J. Aircraft, Vol. 12, No. 9, 1975

/25/ Snel, H.: "A Model for the Calculation of the Properties of a Jet in a Three Dimensional Non-Uniform Mainflow", NLR TR 75085 U

/26/ Sauer, G.: "Ein dreidimensionales Singularitätenverfahren zur Berechnung der Strömung um Bypass-Triebwerke", Dissertation, Institut für Luft- und Raumfahrt, TU-Berlin, 1986

/27/ Jakob, H.: "Ein- und Ausgabebeschreibung für das Programm E 1500", MBB-Interner Bericht, Bericht-Nr. TE2-1333, Febr. 1982

/28/ Hilbig, R.: "Transsonischer Flügelentwurf", Forschungsbericht BMFT-FB-W 80-021,Sept. 1980

/29/ Hilbig, R.: "Vom Windkanal zum Großflugzeug", MBB-UT 116-85 Jahrestagung der DGLR, Bonn-Bad Godesberg, 30.9. - 2.10.1985